analytical chemistry

Article

pubs.acs.org/ac

Prototyping of Wrinkled Nano-/Microstructured Electrodes for Electrochemical DNA Detection

Stephen M. Woo,[†] Christine M. Gabardo,[†] and Leyla Soleymani*[,†,‡]

[†]School of Biomedical Engineering and [‡]Department of Engineering Physics, McMaster University, 1280 Main Street W., Hamilton, Ontario L9H 6K9, Canada

ABSTRACT: Biosensing platforms are ideal for addressing the diagnostic needs of resource-poor areas; however, the translation of such systems from the laboratory to the point-of-need has been a slow process. Rapid prototyping methods that enable an application-specific biosensor to be created in a matter of hours from design to fabrication would expedite the clinical and field testing of such systems. Here, we demonstrate a benchtop method based on craft cutting and polymer-induced wrinkling for creating multiplexed electrochemical DNA biosensors. This fabrication method allows multiscale wrinkled electrodes with features in the millimeter to nanometer length scales to be created in a matter of hours. These wrinkled electrodes display an enhanced surface area compared to planar electrodes and are shown to be structurally tunable by changing the film thickness. We demonstrate that structural tunability of these electrodes is translatable to functional tunability as the density of surface-immobilized probe molecules can be manipulated using wrinkled electrodes of different thicknesses. Furthermore, a simple proof-of-concept electrocatalytic DNA biosensor is demonstrated for distinguishing between complementary and noncomplementary oligonucleotides.

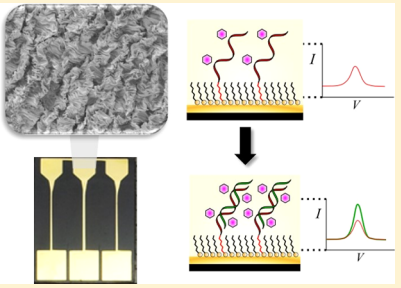

The burden of infectious disease remains a significant public health issue in low- and middle-income countries.[1] Molecular diagnostic methods have the potential to considerably improve infectious disease management in these regions by offering rapid analysis times, strain-level pathogen identification, and effective treatment selection capabilities. However, the commercially available technologies for molecular diagnostics rely on expensive instrumentation, skilled personnel, and basic infrastructure, often unavailable in resource-poor settings.[2,3] The recognition of these limitations has led to tremendous research interest in the development of hand-held biosensors for nucleic acid-based diagnosis of infectious diseases.[2−5] A number of biosensors has been developed that translate nucleic acid hybridization events to electrical,[6] electrochemical,[7] or optical[8] signals. Electrochemical readout in particular has attracted much attention due to its capacity for miniaturization and use of simple self-contained test and measurement instrumentation.[9]

In spite of great promise, the translation of these biosensor technologies from the research lab to the marketplace remains a challenge. Part of the difficulty in technology translation stems from the long period of research and development time required for application-specific device and assay optimization. Standard "top down" microfabrication techniques commonly employed for fabricating chip-based biosensors are suitable for large volume manufacturing, but are time-consuming and costly, making them inappropriate for biosensor prototyping, and testing and validation-level manufacturing.[10]

Rapid and dynamic prototyping methods that allow a new device to be designed and fabricated in a matter of hours are essential for iterative design, optimization, testing, and validation of biosensing assays. Furthermore, using multiscale and tunable electrode materials has enabled electrochemical DNA biosensors to achieve high sensitivities (fM)[11,12] and wide dynamic range.[13,14] A wide array of rapid prototyping methods has been used for fabricating biosensors including soft lithography,[15,16] wax printing,[17,18] screen printing,[19] electrodeposition,[20] and inkjet printing.[21] However, there remains a need for methods suitable for the fabrication of multiscale electrodes with tunable features including contact pads, wires, and reaction areas in the millimeter to nanometer length scale range.

Wrinkled metal films with tunable features in the nanometer to micrometer range have been previously fabricated using a facile and benchtop method that involves heating a thin film coated prestressed polystyrene substrate (PSPS) above its glass transition temperature.[22] Heating the PSPS substrate has a dual effect on the structure of the thin film: it reduces the thin film footprint to 16% of its original value, and it causes the film to wrinkle with a wavelength correlated to the film thickness.[22,23] Furthermore, the patterning of these micro-/nanostructured films in the millimeter and submillimeter length scales is possible using a vinyl shadow mask created by a benchtop craft cutter, making this method ideal for rapid prototyping of biosensors. This method offers a combination of advantages over the above-mentioned rapidly prototyping methods making it ideal for fabricating biosensing devices. It does not rely on masks and molds that cannot be rapidly (<1 h) prototyped; the materials properties such as composition, conductivity, and surface structure can be reproducibly controlled. Materials with

Received: September 27, 2014
Accepted: November 14, 2014

   dx.doi.org/10.1021/ac5036296 | *Anal. Chem.* XXXX, XXX, XXX−XXX

different length scales, having a minimum lateral footprint of 40 μm with micro-/nanoscale features, can be created using a simple and rapid process flow.[23]

In this paper, we use the combination of craft cutting and polymer-induced wrinkling to fabricate a multiplexed array of structurally tunable electrodes for nucleic acid sensing. We present how tunability in the surface structure of wrinkled nano-/microstructured electrodes (WMNEs) is used to control the parameters of the biosensing device including probe density and surface area. Finally, we demonstrate a rapidly prototyped device applied to electrochemical DNA detection.

EXPERIMENTAL SECTION

Chemicals. Potassium chloride (KCl, ≥99.0%), phosphate buffer solution (PBS, 1.0M, pH 7.4), 6-mercapto-1-hexanol (MCH, 99%), 2-mercaptoethanol (MCE, ≥99.0%), hexaammineruthenium(III) chloride (RuHex, 98%), sodium dodecyl sulfate (SDS, ≥99.0%), and saline sodium citrate buffer (SSC), dry blend, were purchased from Sigma-Aldrich (St. Louis, Missouri). Potassium ferricyanide (FiCN, 99.0%) was purchased from Anachemia (Rouses Point, NY). Sulfuric acid (H_2SO_4, 98%), 2-propanol (99.5%), methanol (≥99.8%), and sodium chloride (NaCl, ≥99.0%) were purchased from Caledon Laboratories (Georgetown, Ontario). Ethanol was purchased from Commercial Alcohols (Brampton, ON). Immobilized TCEP Disulfide Reducing Resin was purchased from Thermo Scientific (Rockford, Illinois). Tris-(hydroxymethyl)aminomethane (tris, ≥99.9%) was purchased from BioShop Canada (Burlington, ON). All reagents were of analytical grade and were used without further purification. Milli-Q grade ultrapure water (18.2 MΩ·cm) was used to prepare all solutions and for all washing steps.

Device Fabrication. Sheets of PSPS (Graphix Shrink Film, Graphix, Maple Heights, Ohio) were cleaned by rinsing in 2-propanol and water and were dried under a dry nitrogen stream. The cleaned shrink film was covered with self-adhesive vinyl sheets (FDC 4304, FDC graphic films, South Bend, Indiana). A Robo Pro CE5000-40-CRP vinyl cutter (Graphtec America Inc., Irvine, California) equipped with a CB09UA supersteel blade was used with Adobe Illustrator [v.16.0.3] CAD modeling software (Adobe Systems, San Jose, California) to cut the gold film shapes in the vinyl. The cut vinyl was peeled away with tweezers to leave windows to the PSPS surface through the vinyl mask. The masked shrink film surface was coated by radio frequency sputtering with gold from a 99.999% purity gold target (LTS Chemical Inc., Chestnut Ridge, New York) using a Torr Compact Research Coater CRC-600 manual planar magnetron sputtering system (New Windsor, New York). After sputtering, the remaining vinyl was removed with tweezers, and the shrink film devices were rinsed in 2-propanol and water. The devices were then shrunk on aluminum boats for 3 min at 160 °C. The devices were again rinsed with 2-propanol and water.

SEM Characterization. SEM images of the planar and wrinkled gold electrodes were obtained using a JEOL JSM-7000S scanning electron microscope with an accelerating voltage of 2 kV, working distance of 6 mm, and low probe current.

Preparation of DNA Oligonucleotides. Synthetic oligonucleotides were purchased from Integrated DNA Technologies (IDT, Coralville, Iowa). The sequences used were as follows: PLZD (thiolated probe strand: 5′-[thiol-C6]-CTG GCC GTC GTG GCC CGC AC-3′), F-PLZD (fluorescent, thiolated probe strand: 5′-[thiol-C6]-CTG GCC GTC GTG GCC CGC AC-[6-FAM]-3′), TLZD (complementary target strand: 5′-GTG CGG GCC ACG ACG GCC AG-3′), and T4 (noncomplementary target strand: 5′-TTT TTT TTT TTT TTT TT-3′). The [thiol-C6] modification represents a 5′ hexanethiol, and [6-FAM] represents 3′ 6-carboxyfluorescein.

Prior to use, 5′ disulfide groups of the PLZD and F-PLZD probe strands were reduced through the following procedure. A 100 μL aliquot of TCEP immobilizing slurry was centrifuged and decanted, leaving approximately 50 μL of the gel. A 50 μL solution of 500 μM SH-DNA in 25 mM NaCl and 25 mM PBS (pH 7.4) was added to the gel and left to incubate in darkness at room temperature for 1 h to cleave the disulfide bonds in a reduction reaction. The mixture was then centrifuged in a Nanosep 100 K Omega centrifugal device (Pall Corporation, Port Washington, New York) for 1 min at 12 100*g*, and the filtrate was discarded. 100 μL of buffer containing 1.0 M NaCl and 10 mM PBS (pH 7.4) was centrifuged through the device for 5 min at 12 100*g* to elute the thiolated DNA. The filtrate was recovered, and the absorbance was measured using a spectrophotometer at 260 nm to quantify the concentration of recovered DNA. Reduced PLZD and F-PLZD probe DNA was diluted to 5 μM in 1.0 M NaCl and 10 mM PBS (pH 7.4) to prepare the immobilization buffer (IB).

When performing experiments involving coimmobilization of probe DNA with MCH, an additional filtration step was performed to remove the MCH which resulted from the cleavage of thiolated DNA disulfide bonds. After the DNA was eluted through the Nanosep 100 K Omega column, the eluted DNA solution was spun through a second column, a Nanosep 3K Omega centrifugal device (Pall Corporation, Port Washington, New York) for 15 min at 5000*g*, and the filtrate was discarded. 100 μL of IB was spun through this second column for 15 min at 5000*g* to remove any remaining MCH. Finally, retained DNA was collected in 75 μL of IB. IB solutions were prepared at varying ratios of the two molecules' concentrations such that their combined concentration was 5 μM.

Deposition Characterization with Fluorescent Probes. For experiments characterizing probe deposition, the devices were first wetted with 2-propanol and then IB containing F-PLZD was deposited on fluorescence devices consisting of 2 mm × 2 mm squares of wrinkled or planar gold films on polystyrene. A 5 μL droplet of F-PLZD IB was deposited on these devices in a dark humidity chamber for a specified length of time. Probe deposition was terminated by rinsing the devices in a buffer containing 25 mM NaCl and 25 mM PBS, and then, a backfill was performed by transferring devices into wells containing 200 μL aqueous solutions of 1 mM MCH for 1 h to remove nonspecifically bound probes that were weakly associated with the gold surface. Finally, the devices were washed in ultrapure water and transferred to individual wells in a 96-well black, transparent-bottom plate (Becton, Dickson and Company; Franklin Lakes, NJ) containing 200 μL aqueous solutions (pH 7.4) of 12 mM MCE in 0.3 M PBS for at least 18 h to competitively displace the surface-bound F-PLZD into solution. The devices were then carefully removed, and a plate reader (Tecan Infinite M1000 PRO microplate reader,Tecan Trading AG, Männedorf, Switzerland) was used to measure fluorescence from each well. Fluorescence intensity was used to calculate the density of F-PLZD on the surface of each device. Each condition was performed with devices in triplicate.

dx.doi.org/10.1021/ac5036296 | Anal. Chem. XXXX, XXX, XXX−XXX

Electrochemical Measurements. All electrochemical measurements were performed using a CHI 660D electrochemical workstation (CH Instruments, Austin, Texas). A reference electrode of Ag/AgCl (1.0 M KCl) and a counter electrode of platinum wire were used with the wrinkled or planar gold working electrodes in a standard 3-electrode setup.

Wrinkled and planar gold electrochemical devices were fabricated with three 2 mm × 2 mm square electrodes per device connected to contact pads using thin gold wires. Each electrode's patterned wire was covered using an insulating, water-insoluble polymer glue. The electroactive surface areas of the wrinkled and planar gold films were quantified using cyclic voltammetry (CV) in a solution of 0.05 M H_2SO_4. Devices were rinsed with 2-propanol and water immediately prior to immersion in H_2SO_4 in order to wet the surface. CV was performed with a scan rate of 0.05 V s^{-1} and a voltage range from 0.0 to 1.5 V. The gold oxide reduction peaks of the resulting cyclic voltammograms were integrated to determine the charge, and the electrochemically active surface area was calculated (surface area = charge/surface charge density) using the surface charge density of a monolayer of gold, 386 μC/cm^2.[23]

DNA Detection. Devices were cleaned by rinsing in 2-propanol and water and subsequently performing CV in H_2SO_4 as previously described. Probe deposition was performed using IB containing PLZD probe DNA and MCH at a combined concentration of 5 μM, 1.0 M NaCl, and 10 mM PBS at room temperature for 4 h and followed with a 1 h MCH backfill. Then, a baseline differential pulse voltammetry (DPV) measurement was taken for each electrode using a 3-electrode system in a scan solution (pH 7.4) of 25 mM NaCl, 25 mM PBS, 1 mM FiCN, and 2 μM RuHex. Wrinkled nano-/microstructured electrodes (WNMEs) with 200 nm gold films were used for hybridization with TLZD DNA (complementary) or T4 (noncomplementary) DNA. Both were suspended in a buffer (pH 7.0) containing 25 mM NaCl, 25 mM PB, and 100 mM $MgCl_2$ and were incubated on the device for 1 h in a dark humidity chamber at 37 °C.

The signal amplitude was calculated as the peak current of the DPV curve minus the background current. The change in signal amplitude was calculated by finding the difference between the signal amplitude before and after target incubation and dividing this difference by the signal amplitude before target incubation.

RESULTS AND DISCUSSION

Fabrication of Wrinkled and Planar Gold Electrodes. Our vision was to develop a rapid and inexpensive prototyping method for creating an electrochemical nucleic acid sensor that consisted of a multiplexed array of multiscale electrodes. Electrodes that combine tunability in multiple length scales are necessary for creating ultrasensitive and miniaturized biosensors. Previous reports have shown that the detection limits of DNA biosensors strongly depend on the submicrometer- and nanoscale texturing of the electrode surfaces.[13] Furthermore, submillimeter- and millimeter-scale patterning is required for creating the electrodes' wiring, reaction areas, and contact pads. To engineer electrodes of the required combination of length scales, we developed a lithography-free process combining craft-cutting, vinyl lift-off, and polymer-induced thin film wrinkling (Figure 1a).

The electrode pattern was designed using a computer aided design (CAD) program and was cut into a self-adhesive vinyl mask immobilized on PSPS substrate using a craft cutter (Figure 1a-i–iv). A thin film of gold of controlled thickness (20–200 nm) was sputtered onto the masked devices, and the vinyl mask was then lifted off to reveal the desired gold pattern on the PSPS sheet (Figure 1a-v,vi). To complete the fabrication of wrinkled electrodes, these patterned PSPS substrates were heated to 160 °C. Device heating was performed to serve a dual purpose: to enable miniaturization by shrinking the device area by 84% and to induce controllable wrinkling on the electrode surfaces. Previous reports demonstrated that biaxial shrinking of the substrate caused the adhered gold film to buckle and wrinkle. The size of the resulting wrinkles was shown to depend on the film thickness, with thinner films resulting in wrinkles with a higher spatial frequency.[23] Figure 1b displays the photograph of the devices before (left) and after shrinking.

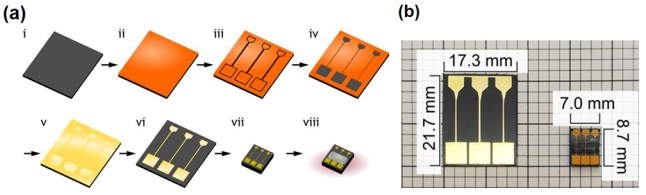

Figure 1. Rapid prototyping of electrochemical biosensors. (a) Schematic drawing demonstrating the fabrication process of WNMEs. (b) Photograph with dimensions of the wrinkled device before and after shrinking.

Characterization of Surface Morphology and Electroactive Surface Area. In order to demonstrate the structural tunability of the wrinkled thin films and to compare their surface texture to planar thin films, we characterized the electrode surfaces using scanning electron microscopy (SEM). Figure 2a demonstrates the SEM images of wrinkled nano-/microstructured electrodes (WNMEs) having gold thicknesses of 20, 100, and 200 nm, as well as of a 200 nm thick planar electrode. Biaxial wrinkling was observed for all film thicknesses, which resulted in nano- and microscale features

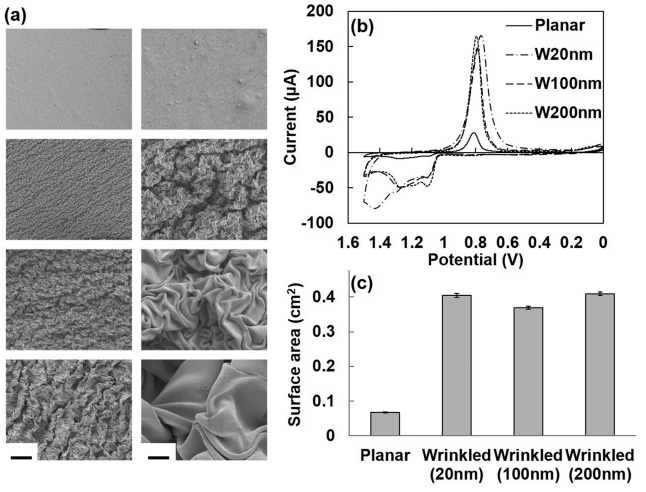

Figure 2. Characterization of wrinkled nano-/microstructured electrodes. (a) Low magnification (left, scale bar represents 20 μm) and high magnification (right, scale bar represents 2 μm) scanning electron micrographs of a planar (top) and WNMEs with 20 nm (row 2), 100 nm (row 3), and 200 nm (row 4) gold films. (b) Cyclic voltammagrams of 2 mm × 2 mm planar electrodes and WNMEs in H_2SO_4. (c) Electroactive surface area calculated from (b).

dx.doi.org/10.1021/ac5036296 | Anal. Chem. XXXX, XXX, XXX–XXX

to be formed. More frequent wrinkles of smaller feature sizes were observed for thinner films, which is consistent with previous reports.[22,23]

Given the three-dimensional structuring present on wrinkled electrodes, we expected WNMEs to present a larger surface area compared to planar electrodes of the same footprint. We used cyclic voltammetery (CV) in sulfuric acid to quantify the solution-accessible gold surface area of planar electrodes and WMNEs of different thicknesses. Wrinkled and planar electrode structures displayed a well-defined redox signature associated with the oxidation of gold and the subsequent reduction of gold oxide (Figure 2b). By measuring the total charge transferred during the reduction of gold oxide (see Experimental Section), we calculated the electroactive surface area of the electrodes (Figure 2c). The surface areas of the planar electrode and WNMEs of 20, 100, and 200 nm thicknesses were measured to be 0.0673 ± 0.0017, 0.4045 ± 0.0051, 0.3692 ± 0.0036, and 0.4094 ± 0.0052 cm^2, respectively. Given that the electrodes were designed with a geometric area of 0.04 cm^2, a surface area enhancement (electroactive surface area/geometric area) of 1.682 ± 0.043, 10.11 ± 0.13, 9.350 ± 0.012, and 10.24 ± 0.13 was measured for planar, 20, 100, and 200 nm electrodes, respectively. The observation that the planar electrode's surface area enhancement is greater than 1 indicates that the sputtered planar surface is not perfectly smooth.[24−26] An approximate 6-fold enhancement was observed in the electroactive surface area of wrinkled electrodes, as compared to that of planar electrodes of equal macroscopic dimensions (Figure 2c). The enhancement in surface area offered by WMNEs and the ease with which they can be fabricated makes them strong candidates for low-cost, high-sensitivity, multiplexed biosensors.

Probe Density Tunability on Wrinkled and Planar Gold Structures (DNA/Thiol Ratio). Hybridization-based biosensors frequently utilize thiol-functionalized capture probe molecules to form self-assembled monolayers on the surface of noble metal electrodes.[2,4,7,26] These surface-immobilized probes, when exposed to their complementary sequence, hybridize and, when combined with a signal transduction method, detect the presence of the captured strand at the surface. Micro-/nanostructured electrodes have been proposed to have greater sensitivities not only due to higher surface areas interacting with the solutions but also through the enhancement of hybridization efficiency (fraction of hybridized probes in a given time) via improved accessibility of target to the probe strands.[7,27] One of the critical parameters in achieving reproducible hybridization efficiencies is precise control over the density of probes at the electrode surface. Past research has shown that optimal probe densities for the greatest hybridization efficiency are significantly below the maximum achievable probe densities for both planar and nanostructured electrodes.[28,29]

To investigate the probe density at the surface of WNMEs and to compare the probe deposition kinetics at the wrinkled and planar electrodes, we used a fluorescence-based probe density quantification method. Thiolated capture probes modified with fluorescence tags were deposited on planar and 200 nm wrinkled electrodes for varying lengths of time (Figure 3a-i). To eliminate the fluorescence contribution of probes attached electrostatically by the backbone rather than by the thiol group, probe deposition was followed by mercapto hexanol (MCH) backfill for 1 h (Figure 3a-ii). The thiolated molecules were desorbed from the device surfaces in solutions

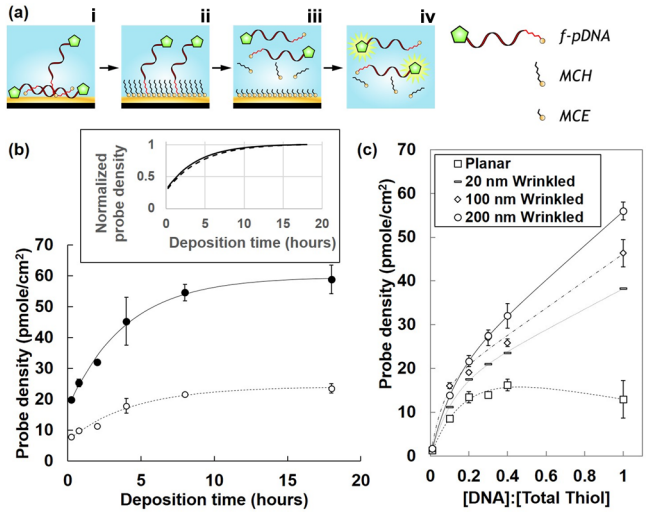

Figure 3. Probe density of WNMEs. (a) Schematic drawing demonstrating the steps involved in quantifying probe density using a fluorescently modified thiolated probe. (b) DNA probe density over time on planar (open circles) and wrinkled 200 nm gold thin films (filled circles); the inset demonstrates the two curves normalized to their highest value at 18 h. (c) DNA probe density on planar and wrinkled gold thin films of varying thicknesses with varying DNA molar fractions in the immobilization buffer, deposited for 4 h.

of mercapto ethanol (MCE) in individual wells of a fluorescence plate (Figure 3a-iii). Fluorescence was measured and the probe density, defined as the moles of the probe molecule (F-PLZD) per cm^2 macroscopic area, was quantified (Figure 3a-iv).

A gradual plateau in probe density was observed for the wrinkled as well as the planar surface morphologies over an 18 h period (Figure 3b). By 4 h, the probe density for all electrode structures had reached at least 75% of that attained after 18 h of deposition. The behavior can be substantiated by theory. The probe density levels off as the surface binding sites become saturated with thiols. The gradual plateau is consistent with what has been seen in past publications.[29−32] Some studies have observed a complete leveling off of probe density after a certain length of time.[30,32] Others report continued increases in probe density, however, at a much slower rate, as seen herein.[29,31]

Wrinkled electrodes had 2.53 times the probe density of planar electrodes; however, the two electrode systems demonstrated very similar deposition kinetics (Figure 3b,inset). An enhancement in probe density is expected for wrinkled electrodes compared to planar electrodes due to the greater gold surface area packed in electrodes of the same macroscopic area. However, the probe density enhancement observed was substantially lower than the 6.1-fold enhancement in surface area measured for WNMEs (200 nm) using electrochemical techniques as demonstrated in Figure 2c. We suspected this discrepancy to be due to the presence of MCH in the immobilization buffer. Due to the dithiol structure of the unreduced DNA probes, the reduction reaction used in their preparation (described in the Experimental Section) leads to the creation of two molecules: the thiolated DNA and MCH. We hypothesize that MCH, having a smaller size and diffusion coefficient compared to DNA, would be adsorbing in greater proportion to the wrinkled surfaces than to the planar surfaces, thus leading to more modest improvements in probe density.

dx.doi.org/10.1021/ac5036296 | Anal. Chem. XXXX, XXX, XXX−XXX

In order to study the effect of the presence of MCH in the immobilization buffer on probe density for wrinkled electrodes, another fluorescence experiment was performed; this time, the deposition step was performed for a period of 4 h and the molar fraction of DNA relative to the total molar concentration of thiolated species in the immobilization buffer was varied. This was achieved by filtration of the MCH product of the reduction process from the immobilization buffer, followed by introduction of varying concentrations of MCH into the buffer and decreasing the concentration of DNA such that the combined concentration of these two thiolated species was 5 μM.

Figure 3c demonstrates that, as the proportion of DNA in the immobilization buffer increased, the probe density on planar electrodes steeply increased until it reached a maximum and plateaued or decreased as the immobilization buffer approached 100% DNA molar fraction. This behavior is in good correspondence with past results seen for planar gold electrodes.[28,33] Keighley et al. observed greater probe densities at 0.5 than at 1.0 DNA molar fraction and hypothesized that the inclusion of MCH during DNA deposition may prevent nonspecific adsorption of DNA, forcing the DNA to extend into the solution (rather than lying flat) and allowing a greater DNA surface immobilization density compared to a case where only DNA was present. A different behavior was observed for wrinkled electrodes of all sputtered thicknesses: as DNA molar fraction increased, the probe density first rose steeply before leveling off into a linear regime (Figure 3c). The broad linear regime is a useful property because it allows for probe density to be easily tuned to very specific values. Past reports have shown that even small differences in probe density can result in large fluctuations in hybridization efficiency.[28] Better control over probe density would facilitate optimization for maximum sensitivity and improve reproducibility for large-scale biosensor fabrication. As demonstrated in Figure 3b, DNA surface density can be controlled by adjusting the deposition time on planar electrodes; however, this is often impractical due to rapid surface saturation and the significant variation in probe densities obtained between experimental trials.[28] Co-immobilization of probe DNA and a diluent thiol allows for an alternate method of probe density tuning and has been explored by multiple authors in the past.[26,28,33−36] However, the linear response of probe density to the DNA mole fraction is a unique property attributed to the wrinkled electrode structure.

In comparison to probe densities observed on planar substrates, the hypothetical 5.5- to 6-fold enhancement predicted by electrochemical surface area measurements was not observed at any molar fraction. The greatest improvement seen in mean probe density was at 1.0 molar fraction for 200 nm thickness wrinkled surfaces, where a 4.3-fold increase was observed. One possible explanation is that there are areas of the gold surface which are electrochemically accessible but not readily accessible by DNA probes. The rate of diffusion of particles through individual pores is understood to be dependent on the diameter of the pores.[37] Gaps between adjacent wrinkles are analogous to pores, which would hinder the diffusion of larger particles. Nano- or microscale narrow gaps in wrinkled structures could potentially allow water molecules and small ions to pass rapidly to cavernous regions in the valleys of wrinkles but not DNA oligonucleotides of significantly larger size within the time scales tested. The observation that the wrinkled electrodes having the largest film thickness of 200 nm showed an increased probe density compared to wrinkled electrodes of lower thicknesses with a similar electroactive surface area (Figure 3b,c) supports this hypothesis. Previous reports have demonstrated that wrinkled films of higher thickness present wrinkles with larger wavelengths compared to thinner films, which would result in the presence of wider gaps on the electrodes.[22] Wider gaps would correspond to less hindrance of diffusion, more areas of the surface being accessible to the DNA molecules, and thus higher obtainable probe densities. Consequently, besides DNA molar fraction, an additional degree of probe density tunability is achievable through control of film thickness of wrinkled electrodes. This is particularly beneficial for optimizing probe density and the resultant hybridization efficiency for hybridization-based biosensors.

Electrocatalytic DNA Detection Using WNMEs at Varying Molar Fractions of DNA. In order to demonstrate the application of the newly developed rapid prototyping technique in electrochemical DNA detection, we employed a previously reported electrocatalytic system[13,27,38,39] to detect DNA hybridization on probe modified wrinkled electrodes. Upon the deposition of probe solutions onto the wrinkled electrodes of 200 nm gold thickness (Figure 4a-i), the devices were scanned by differential pulse voltammetry (DPV) (Figure 4a-ii) to obtain a baseline scan (Figure 4a-iv). Subsequently, the device was exposed to 1 μM of either complementary (TLZD) or noncomplementary (T4) DNA (Figure 4a-v). A second DPV scan was then recorded (Figure 4a-vi) and compared to the baseline scan (Figure 4a-viii) to detect the presence of complementary or noncomplementary targets. The averaged DPV scans (from at least three trials) obtained before and after target incubation are demonstrated in Figure 4b,c for solutions containing complementary and noncomplementary targets, respectively. A detectible signal increase is evident in the presence of complementary targets, while almost no signal change is seen with noncomplementary targets. The same experiment was repeated using planar electrodes, which demonstrated smaller hybridization-induced signal changes compared to wrinkled electrodes (29% compared to 69%) when exposed to complementary targets (Figure 4b,inset). It should be noted that the noncomplementary signal changes (Figure 4c,inset) were similar for both electrode systems. The electrocatalytic system used here was employed to translate the DNA hybridization event to an increase in the measured electrochemical current. As more negative charges are present at the electrode after hybridization, an increased redox current associated with the positively charged RuHex complex is generated. This increase in current is enhanced by the presence of FiCN, which replenishes the oxidized form of RuHex in an electrocatalytic cycle (Figure 4a-iii,vii).

Furthermore, we designed an experiment to optimize the probe density on wrinkled electrodes for maximal electrochemical signal change and minimal background noise. The DPV signals were obtained before and after target incubation for devices modified with different probe solutions, and the percent change in signal amplitude after target incubation was calculated at each DNA molar fraction and is presented in Figure 4d. It is evident from Figure 4d that the signal change generated from incubation with the complementary strands is maximal at the DNA molar fraction of 0.2 and decreases as the molar fraction is increased to 0.4 and 1.0. This is consistent with previous results demonstrating that the hybridization efficiency is optimal at a DNA molar ratio below 1.0, where

dx.doi.org/10.1021/ac5036296 | Anal. Chem. XXXX, XXX, XXX−XXX

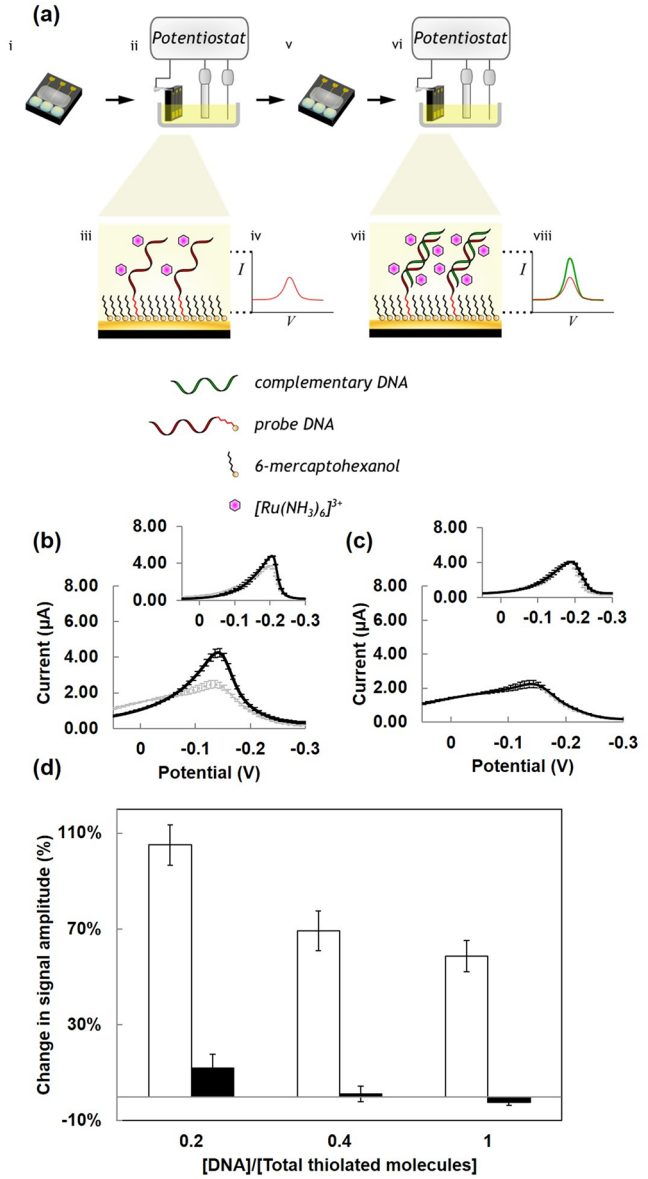

Figure 4. Electrochemical DNA detection using WNMEs. (a) Schematic drawing demonstrating the steps of electrochemical detection. Average electrocatalytic DPV curves of 200 nm thickness wrinkled electrode sensors deposited with a DNA mole fraction of 0.4, before (dotted gray line) and after (solid black line) exposure to 1 μM (b) complementary (TLZD) and (c) noncomplementary (T4) target DNA. The insets of subfigures (b) and (c) show the signals obtained using the planar electrodes. (d) Signal amplitude change after exposure to 1 μM complementary (TLZD, white) and noncomplementary (T4, black) DNA vs mole fraction of DNA to total thiol (DNA + MCH) in the immobilization buffer for 200 nm WNMEs.

steric hindrance and electrostatic repulsion are minimized.[28] It is also seen that the signal change generated from incubating with noncomplementary strands is decreased as the DNA molar fraction is increased from 0.2 to 1.0. Consequently, the optimal preparation condition for WNMEs was at a DNA molar ratio of 0.4, where the highest signal to background ratio (complementary signal change/noncomplementary signal change) was obtained and the complementary and noncomplementary strands were distinguished. Given that varying the DNA molar ratio modifies the probe density, it is evident that the probe density plays an important role in tuning both the hybridization efficiency and signal to background ratio on wrinkled electrodes. The hybridization efficiency is decreased as the probe density is increased, while the signal to background ratio is maximum at a point where the probe density is at an intermediate level of 27 pmol/cm^2.

CONCLUSIONS

We demonstrate a benchtop and rapid prototyping method for developing electrochemical biosensors with a design to fabrication duration of a few hours. We show how tunability in the electrode thicknesses can be translated to controllable micro-/nanostructuring, which allows precise control of the probe density. Furthermore, we demonstrate that, when combined with an electrocatalytic readout system, these electrodes can be used as DNA biosensors. This fabrication method is ideal for developing biosensing prototypes required for optimizing and validating such systems and their translation from the research lab to the point-of-need. A thorough study of the system's limit-of-detection, dynamic range, and ability in distinguishing single base pair mismatches would be important as future work for identifying specific disease management areas to which these electrode systems could be applied.

AUTHOR INFORMATION

Corresponding Author

*E-mail: soleyml@mcmaster.ca.

Author Contributions

The manuscript was written through contributions of all authors. All authors have given approval to the final version of the manuscript.

Notes

The authors declare no competing financial interest.

ACKNOWLEDGMENTS

Financial support for this work was provided by the Natural Science and Engineering Research Council (NSERC), Canada Foundation for Innovation (CFI), Ontario Ministry of Research and Innovation, and Grand Challenges Canada. The electron microscopy research described in this paper was performed at the Canadian Centre for Electron Microscopy at McMaster University, which is supported by NSERC and other government agencies.

REFERENCES

(1) Pinheiro, P.; Mathers, C. D.; Krämer, A. In *Statistics for Biology and Health*; Krämer, A., Kretzschmar, M., Krickeberg, K., Eds.; Springer: New York, 2010; pp 3−21.
(2) Kuralay, F.; Campuzano, S.; Haake, D. A.; Wang, J. *Talanta* **2011**, *85*, 1330−1337.
(3) Wang, J. *Anal. Chim. Acta* **2002**, *469*, 63−71.
(4) Carpini, G.; Lucarelli, F.; Marrazza, G.; Mascini, M. *Biosens. Bioelectron.* **2004**, *20*, 167−175.
(5) Sassolas, A.; Leca-Bouvier, B. D.; Blum, L. *J. Chem. Rev.* **2008**, *108*, 109−139.
(6) Star, A.; Tu, E.; Niemann, J.; Gabriel, J.-C. P.; Joiner, C. S.; Valcke, C. *Proc. Natl. Acad. Sci. U. S. A.* **2006**, *103*, 921−926.
(7) Li, F.; Han, X.; Liu, S. *Biosens. Bioelectron.* **2011**, *26*, 2619−2625.
(8) Yao, X.; Li, X.; Toledo, F.; Zurita-Lopez, C.; Gutova, M.; Momand, J.; Zhou, F. *Anal. Biochem.* **2006**, *354*, 220−228.
(9) Wang, J. *Biosens. Bioelectron.* **2006**, *21*, 1887−1892.
(10) Sharma, H.; Nguyen, D.; Chen, A.; Lew, V.; Khine, M. *Ann. Biomed. Eng.* **2011**, *39*, 1313−1327.
(11) Akhavan, O.; Ghaderi, E.; Rahighi, R. *ACS Nano* **2012**, *6*, 2904−2916.

(12) Hu, K.; Lan, D.; Li, X.; Zhang, S. *Anal. Chem.* **2008**, *80*, 9124−9130.
(13) Soleymani, L.; Fang, Z.; Sargent, E. H.; Kelley, S. O. *Nat. Nanotechnol.* **2009**, *4*, 844−848.
(14) Soleymani, L.; Fang, Z.; Lam, B.; Bin, X.; Vasilyeva, E.; Ross, A. J.; Sargent, E. H.; Kelley, S. O. *ACS Nano* **2011**, *5*, 3360−3366.
(15) Kumar, S.; Kumar, S.; Ali, M. A.; Anand, P.; Agrawal, V. V.; John, R.; Maji, S.; Malhotra, B. D. *Biotechnol. J.* **2013**, *8*, 1267−1279.
(16) Jung, J.; Chen, L.; Lee, S.; Kim, S.; Seong, G. H.; Choo, J.; Lee, E. K.; Oh, C.-H.; Lee, S. *Anal. Bioanal. Chem.* **2007**, *387*, 2609−2615.
(17) Martinez, A. W.; Phillips, S. T.; Whitesides, G. M.; Carrilho, E. *Anal. Chem.* **2010**, *82*, 3−10.
(18) Lu, J.; Ge, S.; Ge, L.; Yan, M.; Yu, J. *Electrochim. Acta* **2012**, *80*, 334−341.
(19) Tudorache, M.; Bala, C. *Anal. Bioanal. Chem.* **2007**, *388*, 565−578.
(20) Mohanty, U. S. *J. Appl. Electrochem.* **2010**, *41*, 257−270.
(21) Komuro, N.; Takaki, S.; Suzuki, K.; Citterio, D. *Anal. Bioanal. Chem.* **2013**, *405*, 5785−5805.
(22) Fu, C. C.; Grimes, A.; Long, M.; Ferri, C. G. L.; Rich, B. D.; Ghosh, S.; Ghosh, S.; Lee, L. P.; Gopinathan, A.; Khine, M. *Adv. Mater.* **2009**, *21*, 4472−4476.
(23) Gabardo, C. M.; Zhu, Y.; Soleymani, L.; Moran-Mirabal, J. M. *Adv. Funct. Mater.* **2013**, *23*, 3030−3039.
(24) O'Dwyer, C.; Gay, G.; Viaris De Lesegno, B.; Weiner, J. *Langmuir* **2004**, *20*, 8172−8182.
(25) Golan, Y.; Margulis, L.; Rubinstein, I. *Surf. Sci.* **1992**, *264*, 312−326.
(26) Ferrario, A.; Scaramuzza, M.; Pasqualotto, E.; De Toni, A.; Paccagnella, A. *J. Electroanal. Chem.* **2013**, *689*, 57−62.
(27) Bin, X.; Sargent, E. H.; Kelley, S. O. *Anal. Chem.* **2010**, *82*, 5928−5931.
(28) Keighley, S. D.; Li, P.; Estrela, P.; Migliorato, P. *Biosens. Bioelectron.* **2008**, *23*, 1291−1297.
(29) Herne, T. M.; Tarlov, M. J. *J. Am. Chem. Soc.* **1997**, *119*, 8916−8920.
(30) Steel, A. B.; Herne, T. M.; Tarlov, M. J. *Anal. Chem.* **1998**, *70*, 4670−4677.
(31) Peterson, A. W.; Heaton, R. J.; Georgiadis, R. M. *Nucleic Acids Res.* **2001**, *29*, 5163−5168.
(32) Demers, L. M.; Mirkin, C. A.; Mucic, R. C.; Reynolds, R. A.; Letsinger, R. L.; Elghanian, R.; Viswanadham, G. *Anal. Chem.* **2000**, *72*, 5535−5541.
(33) Steichen, M.; Buess-Herman, C. *Electrochem. Commun.* **2005**, *7*, 416−420.
(34) Boozer, C.; Chen, S.; Jiang, S. *Langmuir* **2006**, *22*, 4694−4698.
(35) Henry, O. Y. F.; Perez, J. G.; Sanchez, J. L. A.; O'Sullivan, C. K. *Biosens. Bioelectron.* **2010**, *25*, 978−983.
(36) Cederquist, K. B.; Golightly, R. S.; Keating, C. D. *Langmuir* **2008**, *24*, 9162−9171.
(37) Malone, D. M.; Anderson, J. L. *Chem. Eng. Sci.* **1978**, *33*, 1429−1440.
(38) Gasparac, R.; Taft, B. J.; Lapierre-Devlin, M. A.; Lazareck, A. D.; Xu, J. M.; Kelley, S. O. *J. Am. Chem. Soc.* **2004**, *126*, 12270−12271.
(39) Lapierre, M. A.; O'Keefe, M.; Taft, B. J.; Kelley, S. O. *Anal. Chem.* **2003**, *75*, 6327−6333.

dx.doi.org/10.1021/ac5036296 | *Anal. Chem.* XXXX, XXX, XXX−XXX